GROWTH AND STRUCTURE OF WC/Si MULTILAYER X-RAY MIRROR

Y.P. Pershyn, V.S. Chumak, I.G. Shypkova, V.V. Mamon, A.Yu. Devizenko, V.V. Kondratenko, M.V. Reshetnyak, E.N. Zubarev
National Technical University «Kharkiv Polytechnic Institute», Kharkov, Ukraine
E-mail: persh@kpi.kharkov.ua

WC/Si multilayer X-ray mirrors (MXMs) with nominal layers thicknesses of 0.2…30.3 nm (periods: 0.7…38.9 nm) were deposited by direct current magnetron sputtering and studied by X-ray diffraction and cross-sectional transmission electron microscopy (TEM). Carbide and silicon layers are amorphous throughout the studied thickness range. The WC layers interact with Si layers with formation of tungsten silicides (WSi_2, W_5Si_3) and silicon carbide in as-deposited state. The bottom interlayer (WC-on-Si) consists of two subzones of approximately equal thickness. An estimation of the thickness, density, and composition of all layers is made. Based on the experimental data, a five-layer model of the WC/Si MXM structure is suggested.

PACS: 61.05.cm, 61.43.Dq, 68.65.Ac, 41.50.+h, 07.85.Fv

1. INTRODUCTION

Rapid progress in the multilayer X-ray mirror (MXM) manufacturing for the last two decades brought to variety of their applications in science and technology. Some of the applications are: microscopy; astrophysics; devices for synchrotron radiation, plasma physic, X-ray lithography etc. MXM is an optical element meant to reflect, focus, polarize and disperse the X-rays. Particular W/Si-based MXMs become widespread because of a wide range of working wavelength (0.7…3.1 and 12.3…25 nm). Presence of different kind of structural defects, such as mixed interlayers, interfacial roughness etc., disadvantages these MXMs. That is why identification and reduction of these defects are actual to increase the efficiency of W/Si MXM.

The aim of the work is to reduce the level of mixing between W and Si layers during the deposition process by replacing W layer with WC ones. We hope that interaction of tungsten and silicon during deposition of WC onto Si-layers will be decreased due to the presence of carbon. So interfacial interaction in multilayer system WC/Si is studied in this work as a first step to improve the efficiency of W/Si-based MXMs.

2. METHODS

Multilayer mirrors were fabricated by DC magnetron sputtering. During each experimental run the discharge currents for tungsten carbide (WC) and silicon magnetrons and Ar pressure in the vacuum chamber maintained constant, these provided the steadiness of deposition rates for both components. The deposition rates for WC and Si were 0.17 and 0.51 nm/s, correspondingly. Periods of MXMs were in the range from 0.7 to 39 nm.

MXMs were deposited onto substrates of polished silicon wafers and float glass having RMS surface roughness of 0.3…0.5 nm. The plates of WC and Si ~ 100 mm in diameters with a purity of 99.5 and 99.99% correspondingly were used as targets. The distance between a magnetron surface and the substrate was ~ 30 mm.

Multilayer samples were characterized at grazing angles of incidence using small-angle X-ray diffractometer DRON-3M assembled with a single crystal (110) Si monochromator. In combination with a 0.1-mm slit that provided a selection of Cu$K\alpha_1$-line only from the spectrum generated by an X-ray tube with a copper anode. Phase analysis was performed in Cu$K\alpha$-radiation at another diffractometer contained graphite analyzer.

Cross-sections of Mo/Si MXMs were studied in transmission electron microscope PEM-U at accelerating voltage of 100 kV. The images were shot with a line resolution of better than 0.2 nm (atomic planes).

3. RESULTS

For X-ray study we produced 18 separate multilayer samples on different substrates with different periods (*d*) and accordingly the thicknesses of WC layers. Periods values were successively changed from sample to sample in the range of 0.7…14.7 nm at the expense of varied time (τ) of substrate exposure above respective magnetron. Deposition times or both components were equal in every single experiment. We varied amount of periods (m) in each sample of X-ray series from 310 to 17 in order to have equal thicknesses of the multilayers. So overall thickness of multilayer coating in each sample were $m \times d \approx (234 \pm 1)$ nm.

3.1. X-RAY SPECTROMETER SURVEY

We controlled the thickness (*t*) of each layer by varying the stopover time (τ_{fix}) of the sample above the magnetron since we kept the identical deposition rate of each component in each experiment. However, there is also an additional amount of substance deposited during the motion of the substrate over the magnetrons, i. e. a layer deposited while moving the substrate from one magnetron to another. To account for this quantity of the substance, we introduce the notion of approach-departure time, $\tau_{a/d}$, which is equal to the ratio of the layer thickness sputtered onto the moving substrate to the deposition rate of this component in the center of the magnetron. To determine $\tau_{a/d}$ we used an X-ray spectrometer SPRUT. In this spectrometer, the characteristic radiation of W-$L\alpha$ is excited by an X-ray tube with a silver anode in each WC layer placed in the irradiation region, and therefore the amount of tungsten in the samples can be judged from the intensity of W-$L\alpha$ line. In this study, we used the reduced intensity of W-$L\alpha$,

equaled to the intensity of the tungsten characteristic line from the entire sample, divided by the number of periods in this sample.

Fig. 1 shows a dependence of the reduced intensity of the W-$L\alpha$ tungsten line on the fixed sputtering time (τ_{fix}). As it can be seen from the figure, the experimental points fit well on the straight line, which indicates the constancy of the deposition rate of WC and the good reproducibility of the deposition conditions in this series. A straight line drawn through the experimental points does not intersect the origin of coordinates. This is because in this graph we did not take into account the deposition of the material during the substrate motion, at least in the abscissa data. Since, as we indicated above, the intensity of the characteristic tungsten line is a measure of the tungsten amount in the samples, the intersection of the straight line in Fig. 1 with the "X" axis gives the sought approach-departure time, i. e. $\tau_{a/d} = (0.72 \pm 0.06)$ s. Thus, adding this value to the τ_{fix}, we can determine the overall deposition time (τ) and, knowing the deposition rate (DR), the nominal thickness of the layers (t_{WC}, t_{Si}) in each sample.

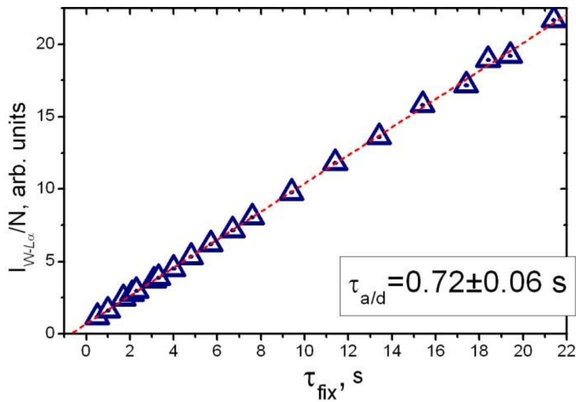

Fig. 1. Dependence of the reduced intensity of W-$L\alpha$ radiation excited in WC/Si MXMs on the stopover time of tungsten carbide (silicon) deposition

3.2. SMALL-ANGLE X-RAY SURVEY

Each multilayer sample was measured at X-ray diffractometer ($\lambda = 0.154$ nm) within the angle range of $2\theta < 20°$. Fig. 2 shows an example of the obtained and processed diffractogram. The figures designate the reflection orders (n). Here 16 reflection orders are visible, indicating, on the one hand, a good reproducibility of the deposition processes (according to the Bragg equation, the periodicity of $d/n \sim 0.53$ nm is observed in the sample), and on the other hand, a low interlayer roughness ($\sigma < 0.26$ nm [1]). The period value was determined with consideration for the refraction in the sample and using all the diffraction peaks. The high accuracy in the period determination also indicates the good periodicity. Although in this particular case the accuracy of the period measurement is extremely high, in general for all samples having at least three diffraction maxima ($d > 1.5$ nm), the error in determining the period did not exceed ±0.002 nm.

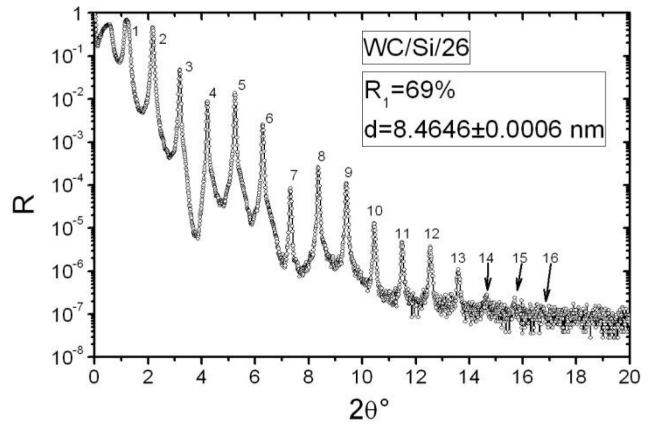

Fig. 2. Example of a small angle diffractogram of WC/Si MXM with 26 periods and a period d ~ 8.46 nm

Both tungsten and carbon under the conditions of WC-target sputtering move predominantly not in molecules, but atomically [2]. Deposited onto the surface of a silicon layer, they can interact with it. In order to estimate the extent of the layers interaction in the WC/Si MXMs, we have plotted mirror period as a function of the deposition time, τ, taking into account the approach-departure time (see Fig. 1). If the deposition rates are constant, we should obtain a linear dependence of $d = f(\tau)$, since the slope ratio in this graph determines the deposition rate. A straight line drawn through the last seven points gives a combined deposition rate equal to DR = (0.689±0.002) nm/s, which corresponds to the sum of the previously measured component deposition rates. A small error in the deposition rate (~ 0.3%) indicates the constancy of the deposition rate for large-period MXMs. However, the deposition rate, determined for the small-period samples, is much smaller. It is (0.560±0.001) nm/s (± 0.2%) for the first three points, which is ~ 19% less than for samples with larger periods. An increase in the number of points in the approximation leads to increasing the error and approaching values of the deposition rates determined at the extreme ends of Fig. 3. The nonlinearity observed in Fig. 3 can be related either to resputtering one of the components, for example, silicon, or to the interaction of both components at the interfaces during the stage of layer deposition. Below we will consider both of these options in order to find out the main reason for this behavior.

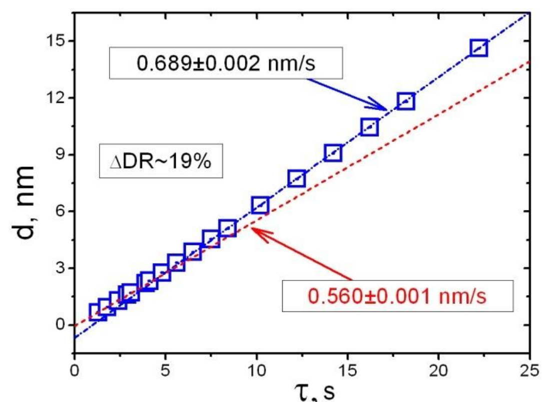

Fig. 3. Dependence of the MXM period on the deposition time of individual layers

Table 1

Calculation results of chemical reactions for molar volumes of components (one formula unit implies the participation of one mole of a substance)

No	Reaction	V, cm^3	$-\Delta V$, cm^3	$-\Delta V$, %	$-\Delta V/V_{WC}$
1	$WC+3Si=WSi_2+SiC$	12.48+36.13=25.95+12.49	10.17	20.9	0.815
2	$5WC+8Si=W_5Si_3+5SiC$	62.38+96.35=69.54+62.46	26.73	16.8	0.429
3	$7WC+9Si=W_2C+W_5Si_3+6SiC$	87.33+108.39=22.08+69.54+74.95	29.15	14.9	0.334
4	$3WC+4Si=W_2C+WSi_2+2SiC$	37.43+48.17=22.08+25.95+24.98	12.59	14.7	0.336
5	$WC+2Si=WSi_2+C$	12.48+24.09=25.95+5.34	5.28	14.4	0.423
6	$2WC+Si= W_2C+SiC$	24.95+12.04=22.08+12.491	2.419	6.5	0.097
7	$3WC+2Si=W_2C+WSi_2+2C$	37.43+24.08=22.08+25.95+10.68	2.8	4.6	0.075
8	$5WC+3Si=W_5Si_3+5C$	62.38+36.13=69.54+26.69	2.28	2.3	0.037
9	$7WC+3Si=W_2C+W_5Si_3+6C$	87.33+36.12=22.08+69.54+32.04	-0.21	-0.1	-0.002
10	$2WC+Si= W_2C+C+Si$	24.95+12.04=22.08+5.34+12.04	-2.47	-6.7	-0.099

We considered possible reactions between the components that compose the deposited substance (WC+Si) in order to estimate reaction products appeared as a result of the WC and Si interaction. There were examined 10 reactions involving the initial components WC and Si. As final products we took two tungsten silicides (WSi_2 and W_5Si_3), tungsten carbide W_2C, silicon carbide SiC and pure element C. We used tabulated data for the densities of substances in the bulk state for calculation. The calculations presented in Tabl. 1 are made for the molar volumes of each substance. Two penultimate columns also contain data on volume changes (positive values – shrinkage, negative – increase in volume).

As can be seen from Tabl. 1, the majority of the presented reactions should proceed with volume shrinkage in the reaction products. Since our experiments also demonstrate shrinkage in volume, we have omitted the reactions 9 and 10 from the further consideration. In addition, volume changes, as we determined above, can reach 19%. Formally, only the first reaction (shrinkage 20.9%, penultimate column) satisfies this condition, with the formation of WSi_2 and SiC at the interfaces. However, taking into account the fact that the film densities can differ noticeably from massive materials, we have left the first five reactions only for further consideration.

Assuming that the volume shrinkage in thin layers during the deposition is caused by the interaction of the components, we estimated the shrinkage (Δd) as the difference between the expected period (d_{expec}) and the experimental (d_{exper}) by the formula:

$$\Delta d = d_{expec} - d_{exper} = DR \times \tau - d_{exper},$$

with DR is overall deposition rate, τ is overall deposition time.

Plot of the experimental shrinkage versus the WC layer thickness in the period is shown in Fig. 4. To plot this dependence, we used data of the deposition rates for WC (0.171 nm/s) and Si (0.518 nm/s) obtained earlier in a separate experiment. As it can be seen from the plot, the shrinkage increases with thickness and reaches a maximum value near ~ 0.7 nm. The growth process can be conditionally divided into four regions: (I) t_{WC}=0.2…0.4 nm, where the highest increment in Δd is observed ($\Delta d/t_{WC} \sim 0.76$); (II) t_{WC} = 0.4…0.7 nm, where the stunted growth in Δd ($\Delta d/t_{WC} \sim 0.44$) is observed; (III) t_{WC} = 0.7…1.4 nm, where the intermediate value of Δd ($\Delta d/t_{WC} \sim 0.24$) is observed, and (IV) t_{WC} > 1.4 nm, where the shrinkage achieves a saturation (Δd ~ (0.64±0.02) nm). The first 3 regions may correspond to intermixed sublayers with different extents of interaction of WC with silicon. Formally, in terms of X-ray optics, they must be referred to strongly absorbing (or strongly scattering) layers, and they should be accounted either as a part of the WC layer or as replacing layers (if the entire WC layer reacts with Si). Henceforward, we shall call these zones as "W-containing" to indicate a different extent of tungsten carbide interaction with its environment.

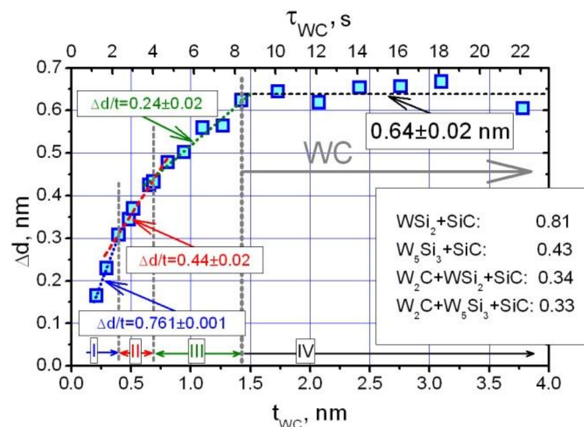

Fig. 4. Graph of the experimental volume shrinkage (Δd) versus the thickness of the WC (t_{WC}) layer in the period

To make a choice in favor of a particular compound to be formed at interfaces, we also calculated the ratio of the volume change to the WC volume for each reaction (see Tabl. 1, last column). For the first and second reactions, these values are 0.81 and 0.43, respectively. Comparing these quantities to the data obtained in Fig. 4, it can be concluded that in the region I the majority of the components (> 90%) should react with the formation of WSi_2 and SiC. In the region II, W_5Si_3 can be formed instead of WSi_2. In the region III, we cannot unambiguously indicate which of the reactions can take place, since if we assume that the reaction can proceed partially, then either one of the five first reactions or all five reactions can formally fit to the observed increase in Δd. We do not exclude that in this case (region III)

WC can react with silicon partially, remaining as a WC compound in the film. However, we can say for sure that at $t_{WC} > 1.4$ nm (see region IV in Fig. 4) there is a WC in the tungsten-containing layer that does not react with the silicon layer. Moreover, it should be in the middle of the W-containing layer.

3.3. CROSS-SECTIONAL TEM STUDY

For the TEM study, a cross-section of a special sample on a silicon substrate was prepared. It was located in the microscope so that we can view its image along the layers. The sample consisted of 14 multilayer stacks, the periods of which were successively varied by changing the deposition time of each of the components. Since within the whole coating the deposition rates of WC and Si did not change, then the nominal ratio of the component thicknesses in each stack was kept constant ($t_{Si}/t_{WC} \sim 3$). At first, the stacks with the smallest periods were deposited onto the substrate in order to mitigate the roughness development effect observed in large-period MXMs.

Fig. 5 represents cross-sectional TEM images of different areas for multilayer stacks with the smallest periods [(*a*) $d \sim 1.8$ nm, (*b*) $d \sim 3.5$ nm] and the largest period [(*c*) $d \sim 38.9$ nm]. The dark stripes correspond to the WC layers, and the light stripes correspond to the Si layers. There is no contrast associated with interlayer interaction at the interfaces. Fig. 5,d,e shows the selected-area electron diffraction (SAED) pattern of a multilayered sample and its densitogram taken at the center of the SAED pattern (see Fig. 5,d) in the horizontal direction. There observed 3 halos there: 1) with $d_1 \sim 0.37$ nm, if we estimate it using the Bragg formula (denoted as r_1); 2) $d_2 \sim 0.19$ nm (r_2), and 3) $d_3 \sim 0.12$ nm (r_3). The SAED pattern shows that the multilayered sample is basically amorphous, though the proximity of d_2 and d_3 to d_1/n indicates that some of the WC layers (especially thickest ones) may be in the nanocrystalline state.

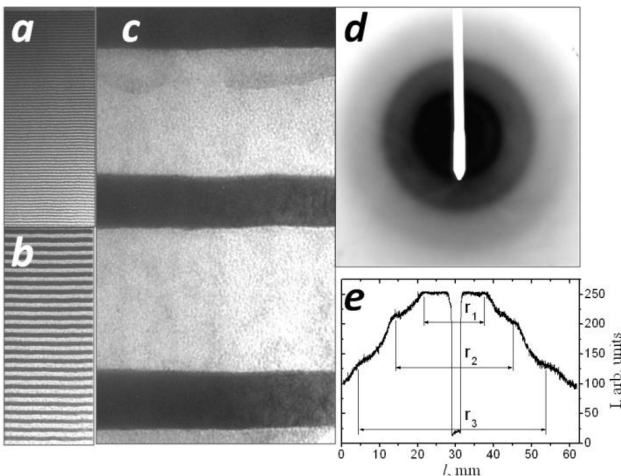

Fig. 5. Cross-sectional TEM images of various WC/Si multilayer stacks with periods of d = 1.8 nm (a), d = 3.5 nm (b) and d = 38.9 nm (c). SAED pattern and densitogram taken horizontally across the center of the pattern are represented in (d) and (e), respectively

We measured the thickness of all layers and periods in each stack, taking into account the image magnification. The measured results as a function of the components deposition time in each stack are shown in Fig. 6,a. All three dependencies are generally nonlinear, and none of them intersect the origin of coordinates. However, after about 27 s, the experimental values fit well the straight lines. From the Fig. 6,a we determined the deposition rates of the components as well as the overall deposition rate by the dependency slopes: $DR_{WC} = (0.17 \pm 0.02)$ nm/s; $DR_{Si} = (0.5 \pm 0.01)$ nm/s (Si), and $DR = (0.68 \pm 0.02)$ nm/s, which match well to each other. This data also accords well with the X-ray measurements and show that the deposition rates of the components can be measured in this way. The dependences of $t_{WC}=f(\tau)$ (triangles) and $t_{Si}=f(\tau)$ (circles) intersect, and at $\tau < 10$ s the thickness of WC layer becomes larger than the thickness of Si layer ($t_{WC} > t_{Si}$), which contradicts the experimental conditions in which the silicon deposition rate is higher.

It is noteworthy that the fraction, β, of W-containing layers in the periods increases and varies from $\beta \sim 0.3$ for the largest periods to $\beta \sim 0.9$ for the smallest at the nominal fraction of $\beta_{nom} \sim 0.25$. Based on this data, we make the final choice in favor of the main reason for the nonlinearity in the dependence $d=f(\tau)$ observed in Fig. 3. For the small-period sample ($d \sim 1.8$ nm), the nominal WC thickness should be ~ 0.53 nm, and actually we have ~1.6 nm. If we assume that the main effect of β distortion is sputtering, then for this stack the silicon thickness should be $1.6 \times 3 = 4.8$ nm, and the period – $4.8+1.6 = 6.4$ nm, while the nominal period should be $(0.17 + 0.51)$ nm/s $\times$ 3.12 s $= 0.68 \times 3.12 \approx 2.12$ nm, i. e. 3 times less. However, if we compare the ratio of the reaction products volume to the initial volume of WC (see Tabl. 1, reaction No 1) with the actual one, than we obtain $(25.95+12.49)/12.48 \sim 3.1$ and $1.6/0.53 \sim 3$, respectively. In other words, the experimental data support the idea of the interlayer interaction.

We can estimate the amount of silicon resputtered during deposition of the WC layer in a different way. The approach/departure time (see subsection 3.1) can be also determined from the data for the small-period MXMs, using the fact that the volume of reaction products in the period is very close to the nominal volume of the silicon layer: the difference is ~ 6% (see Tabl. 1, reaction No 1). In our experiments, the ratio of the nominal deposition rates is close to the ratio of the initial volumes of WC and Si (the difference is ~ 3%), therefore, on one hand, the volume of the reaction products should correspond to the MXMs period (d), and on the other hand, the silicon deposition rate (DR_{Si}) should be ~ 0.94 of the deposition rate measured for small periods. Then the approach/departure time, $\tau^*_{a/d}$, can be calculated by the formula:

$$\tau^*_{a/d} = (d - \tau_{fix} \times DR_{Si})/DR_{Si}.$$

For three MXMs with the smallest periods, where we expect a complete interaction of WC and Si, we get $\tau^*_{a/d} \approx (0.77 \pm 0.03)$ s, i.e. on $\Delta\tau \sim 0.05$ s more than for $\tau_{a/d}$, calculated in section 3.1 with the fluorescent signal from tungsten. If this value is multiplied by the deposition rate of silicon, we get $\Delta t = 0.05 \times 0.562 \approx 0.03$ nm, i. e. this amount is “lacking” in the MXM. In other words, the sputtering effect in a WC/Si multilayer sys-

tem, even if it exists, is negligible in comparison with the interlayer interaction effect.

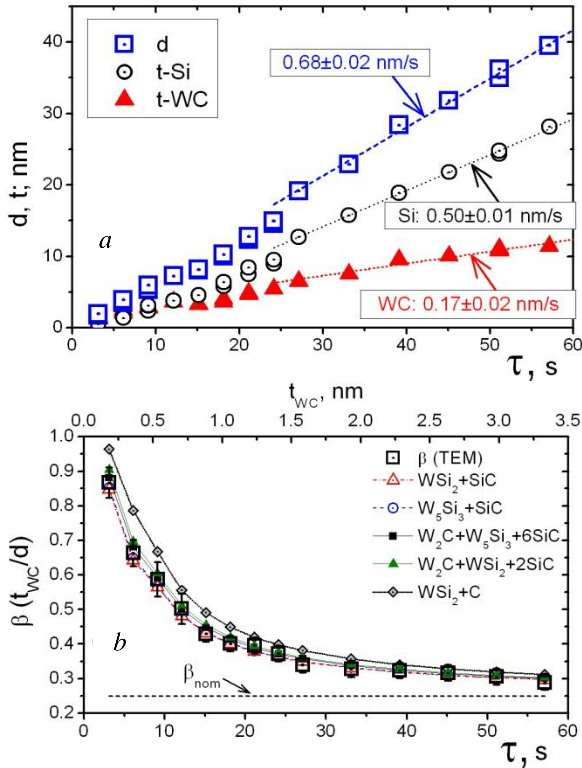

Fig. 6. Dependences of the period of multilayers stacks and layer thicknesses in the corresponding stacks on the deposition time of each layer (a). The experimental fraction (β) of the WC layer in the period (light squares) according to electron microscopy and the calculated fractions for different products of the reaction at the interfaces, depending on the time of individual layer deposition (lower scale) or on the WC layer thickness (upper scale) (b)

We have plotted the dependence of the W-containing layer proportion (β) measured in the cross-sections from the total deposition time of each component (the squares in Fig. 6,b). This fraction reaches ~ 0.9 for the small-period MXMs, as was established earlier, and then decreases with the deposition time (and, correspondingly, with the period and thickness of the layers), asymptotically approaching the nominal value of β_{nom}. Using X-ray data (subsection 3.2) of volume shrinkage for different samples, we calculated the fractions β for various reactions that could be expected in the given multilayer system. These fractions are also plotted in Fig. 6,b. Almost all the calculated fractions are close to the experimental ones, as can be seen from the figure. The exception is the reaction products WSi_2+C, which are significantly higher in the entire data range, especially for $\tau < 20$ s. Therefore, we suggest that this type of interlayer interaction is unlikely.

3.4. X-RAY PHASE ANALYSIS

Samples with nominal WC thicknesses in the range 0.2…3.8 nm (periods $d < 14.7$ nm) were scanned in glancing geometry ($\theta = 1.4°$ is fixed) in the angle range of $2\theta = 15…110°$. Diffractograms for two ultimate samples with thicknesses of WC layer ($t_{WC} \sim 0.21$ nm and $t_{WC} \sim 3.78$ nm) are shown in Fig. 7. As can be seen from the figure, two diffraction maxima are observed in the diffractogram. The width of the maxima is in the range of 5…10°. Such a small number of maxima, as well as their width, indicate the amorphous structure of both layers. The most intense maxima, which are in the region of $2\theta \sim 40°$, are shifted relative to each other by more than 2°, which indicates an additional difference in their structure. The second maxima (near 69°) are not the second orders of reflection, because with an increase in the WC thickness they shift in reverse directions.

Taking into consideration that there are no triple compounds in the W-Si-C-system [3], and that the scattering power of tungsten atoms is at least 25 times higher than for carbon and silicon atoms, the peaks observed in the diffractograms should be related to W-containing layers only, i.e. to tungsten carbides or silicides. Usually the angular position of the most intense line for an amorphous substance is close to the 100% line for crystalline one [4]. In addition, since the crystalline state corresponds to the tightest packing of atoms, then for an amorphous substance, where the atoms are disordered, the average interatomic distance is larger, and the angular position of the most intense maximum in the diffraction pattern should shift slightly toward smaller angles. This is observed in the diffraction pattern (see Fig. 7) with respect to 100% of the line (200) WC_{1-x} [5]. However, it is difficult to unambiguously establish the composition of a substance along a single line, since a 100% line for WSi_2 is at an angle of $2\theta \sim 42.6°$.

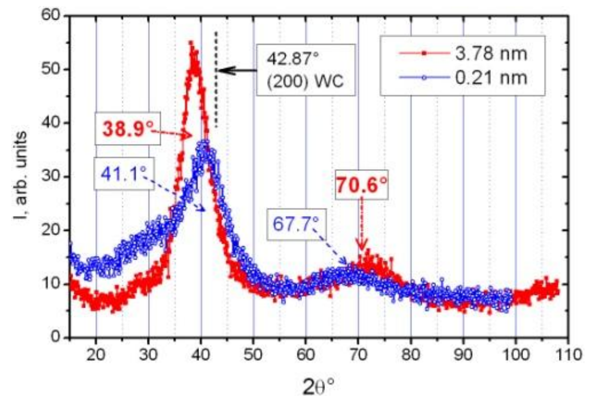

Fig. 7. Phase diffractograms for MXMs with nominal WC thicknesses of 0.21 nm (circles) and 3.78 nm (boxes)

To further detail the structure of the amorphous state, we also made the Fourier transform of the obtained X-ray diffraction patterns in order to construct the radial distribution functions. It was established above (subsection 3.2) that the W-containing layer in the WC/Si MXM can consist of 4 zones. We performed the following manipulations to analyze them. First, we reduced each diffractogram to one period dividing its intensity by the number of periods contained in the particular mirror. Then we successively subtracted the diffractograms from each other for samples located at the boundary of two adjacent sublayers. Thus, we obtained the reduced differential diffractograms characterizing the individual zones only. For example, MXM with a WC thickness of ~ 0.40; ~ 0.69, and ~ 1.42 nm are boundary (see Fig. 4). In multilayer samples with

$t_{WC} > 1.5$ nm, W-containing layers consist of 4 zones (I, II, III, IV), with $t_{WC} < 1.42$ nm they consist of 3 zones (I, II, III), with $t_{WC} < 0.69$ nm – of 2 zones (I, II), etc. Then if we subtract from the given diffractogram for the sample with $t_{WC} \sim 0.69$ nm the diffraction pattern of the sample with $t_{WC} \sim 0.40$ nm, then we obtain a diffraction pattern characterizing zone II only. We carried out the Fourier transformation only for such reduced diffractograms of individual zones.

An example of such a transformation for zone I is shown in Fig. 8. Here we present: (a) the original diffraction pattern for the MXM with $t_{WC} \sim 0.4$ nm (circles) with an indication of the positions for the 100% lines of the tetragonal and hexagonal WSi_2, and the differential diffraction pattern, which is the result of subtraction diffractograms with $t_{WC} \sim 0.40$ nm and $t_{WC} \sim 0.21$ nm (boxes) (see Fig. 8,a); (b) the radial distribution curve of the atoms for the differential diffraction pattern (see Fig. 8,b), in which we determine the radius (r_1) of the first coordination sphere and the coordination number (CN_1), used hereafter as experimental data, and (c) an enlarged image of the first maximum in Fig. 8,b (see Fig. 8,c). The experimental radius of the first coordination sphere and the coordination number were $r_1 = 0.292$ nm and $CN_1 = 5.97$. For comparison, Fig. 8,c shows similar data for hexagonal ($r_1 = 0.298$ nm and $CN_1 = 6$) and tetragonal ($r_1 = 0.231/0.263$ nm and $CN_1 = 4$) WSi_2. Through comparison of the given data, it can be established that zone I basically consists of hexagonal WSi_2. In the W-Si phase equilibrium diagram, the h-WSi_2 phase is high-temperature one [6] and its appearance may be somewhat unexpected, but a similar picture was observed in the Mo/Si MXM in which h-$MoSi_2$ is formed at the interface during the annealing.

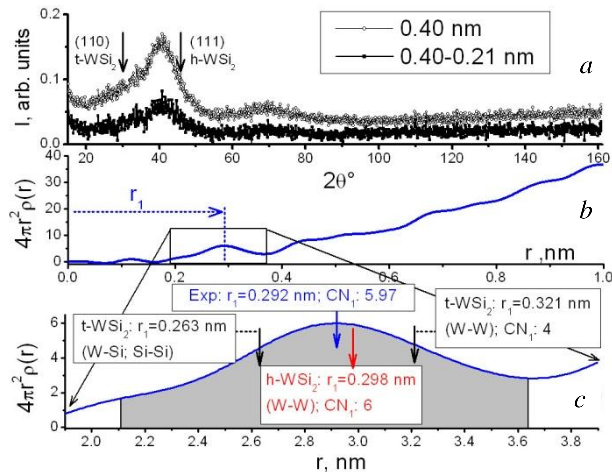

Fig. 8. X-ray diffraction pattern from WC/Si MXM with a nominal WC thickness of $t_{WC} \sim 0.4$ nm (circles) and a differential diffraction pattern (boxes) obtained by subtracting two diffraction patterns from each other for MXM with $t_{WC} \sim 0.4$ nm and $t_{WC} \sim 0.21$ nm to obtain a diffraction pattern from zone I (see Fig. 4) (a). Radial distribution function of atoms for zone I (b). An enlarged image of the region of the first maximum shown in Fig. 8,b (c)

It should be noted that the radii of the first coordination spheres for other W-containing substances (W_5Si_3, W_2C, WC) are not too different from the experimental value of r_1. Meanwhile, the coordination numbers increase noticeably with the content of tungsten from 6 (for 20 at.% W) to 12 (50 at.% W), which makes it possible in most cases to uniquely determine the phase of matter.

We carried out similar manipulations for the remaining zones and established that zone II consists of a tetragonal W_5Si_3; and tungsten carbide (zone IV) is in a configuration close to the cubic one. We could not establish the phase composition of zone III unequivocally, since at least two W-containing substances: silicide (WSi_2 and/or W_5Si_3) and carbide (W_2C and/or WC) can be present in this zone.

3.5. THE MODEL OF WC/Si MXM STRUCTURE

Summing up the data given above, we can build a model of the WC/Si MXM structure. We have established that the bottom interface with respect to WC layer (WC-on-Si one) consists of two subzones: (1) WSi_2 and SiC (adjacent to the Si layer) and (2) W_5Si_3 and SiC (adjacent to the WC layer). The top interface (Si-on-WC one) can consist of a silicide and carbide. Tungsten carbide (WC) can appear at $t_{WC} > 1.5$ nm. Densities of layers and interlayers were estimated from the critical angles by the method we described earlier in [7]. A schematic sketch of the WC/Si MXM structure for $t_{WC} > 1.5$ nm is shown in Fig. 9.

If the WC thickness is less than 1.5 nm, then in the WC/Si MXM W-containing layer will consist of only three, two sublayers or one layer, depending on the tungsten carbide applied thickness. We would like to draw attention to the fact that the “pure” WC layer in the WC deposition process may be formed at $t_{WC} > 0.7$ nm, rather than at $t_{WC} > 1.5$ nm. However, the deposition of the subsequent silicon layer and the interaction with it leads to its “disappearance”.

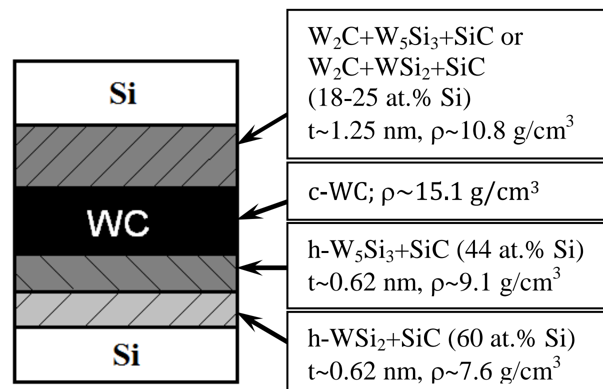

Fig. 9. Schematic sketch of the WC/Si MXM structure for $t_{WC} > 1.5$ nm

3.6. COMPARISON OF OPTICAL CHARACTERISTICS FOR WC/Si AND W/Si MXMs

The determined parameters allow to estimate the optical characteristics of WC/Si MXMs by simulating diffraction curves, and to compare them with the characteristics of the W/Si MXMs. W/Si mirrors are commonly used in material science to analyze the content of light elements (oxygen, sodium, magnesium, aluminum, silicon, etc.) by measuring the intensity of the characteristic

lines of the analyzed elements and comparing them with that for a standard. The period of such MXMs is comparable with the wavelength of the characteristic line and is usually ~ 3 nm. In the mirror with such a period and a fraction of β ~ 0.4, the W-containing layer consists of a two zones for WC/Si MXM (WSi_2+SiC and W_5Si_3+SiC) and one zone for W/Si MXM (WSi_2 [7]). In such a way, the W/Si mirrors should have an advantage, since the W-containing layer (WSi_2 or W_5Si_3) in the WC/Si MXM is "diluted" by the SiC compound with a lower density. The phase roughness was taken as 0.26 nm (WC/Si), as follows from the subsection 3.2, and 0.38 nm (W/Si [7]), i. e. the interfacial roughness of the mirrors under study is almost 1.5 times smaller. The densities of substances, which are approximately 5…7% lower than the tabulated values, were measured by us earlier. The number of periods in both compared MXMs was 101. The calculated optical characteristics for the 5 characteristic lines in the wavelength range 1…2.4 nm are presented in Tabl. 2. In the whole range of wavelengths, the WC/Si MXMs have an advantage only due to a lower interfacial roughness. More smooth interfaces in the WC/Si MXMs compared to W/Si were also observed by other researchers earlier [8]. The advantage of WC/Si is 10…15% (relative units) for all characteristic lines.

For WC/Si MXMs with all zones of the W-containing layer presented, for example, with periods of $d > 6$ nm, the advantage of the WC/Si MXMs over W/Si ones should be even more obvious, since the total thickness of the interlayers in WC/Si MXMs is ~ 2.5 nm, while in the W/Si ones this value reaches ~ 2.8 nm [7].

Table 2

Simulated reflectivities for WC/Si and W/Si MXMs at characteristic lines of light elements

Characteristic line	λ, nm	MXM	R, %
Mg-Kα	0.989	WC/Si	**33.8**
		W/Si	30.0
Na-Kα	1.191	WC/Si	**23.4**
		W/Si	21.4
Cu-Lα	1.334	WC/Si	**20.0**
		W/Si	18.0
Fe-Lα	1.759	WC/Si	**12.2**
		W/Si	10.9
O-Kα	2.36	WC/Si	**6.52**
		W/Si	5.64

CONCLUSIONS

WC/Si multilayer X-ray mirrors prepared by direct-current magnetron sputtering with periods in the range of 0.7…38.9 nm were studied by cross-sectional transmission electron microscopy and X-ray diffractometry. All layers in MXMs are in an amorphous state. The interaction of WC and Si layers with the formation of interlayer zones is found; that manifests in the variation of the fraction of the W-containing layer in a period from 0.29 to 0.87 at a nominal fraction of 0.25. The bottom (WC-on-Si) and top (Si-on-WC) interlayers are close and are ~ 1.22 nm and ~ 1.25 nm, respectively. The bottom interlayers consist of two subzones of equal thickness, consisting predominantly of WSi_2 and SiC (adjacent to Si layers) and W_5Si_3 and SiC (adjacent to W layers). The top interlayers are presumably composed of W_2C+W_5Si_3+SiC and/or W_2C+WSi_2+SiC. Radial distribution functions are constructed to refine the preferred structure types for amorphous layers; they are: hexagonal for both silicides in the bottom interlayers and cubic for WC tungsten carbide. The model of WC/Si MXM construction is proposed consisting of 5 layers. The advantage in the soft X-ray optical characteristics for the WC/Si MXMs is shown in comparison with W/Si MXMs.

ACKNOWLEDGMENTS

YPP acknowledges ISKCON for the help in understanding the place and the meaning of this study.

REFERENCES

1. Y.P. Pershyn, E.N. Zubarev, V.V. Kondratenko, V.A. Sevryukova, and S.V. Kurbatova. Reactive diffusion in Sc/Si multilayer X-ray mirrors with CrB_2 barrier layers // *Appl. Phys. A*. 2011, v. 103, p. 1021-1031.
2. G. Betz, G.K. Wehner. Sputtering of Multicomponent Materials *in Sputtering by Particle Bombardment II* / ed. R. Behrisch. Springer-Verlag, 1983, p. 11-90.
3. F. Goesmann, R. Schmid-Fetzer. Stability of W as electrical contact on 6H-SiC: phase relations and interface reactions in the ternary system W-Si-C // *Materials Science and Engineering*. 1995, v. B34, p. 224-231.
4. Ya. I. Datchuk. *X-ray study of liquid metals*. Lviv: "High school", 1977, p. 47-85.
5. ICDD Power Diffraction File, 1996, Card #20-1316.
6. N.P. Lyakishev. *Phase diagrams of binary metal systems.* M.: "Machine-building", 2000, v. 3, p. 301-302.
7. Y.P. Pershyn, A.Yu. Devizenko, V.V. Mamon, V.S. Chumak, and V.V. Kondratenko. Structure? Phase composition and growth model of amorphous W/Si multilayer X-ray mirrors deposited by magnetron sputtering // *Journal of Surface Physics and Engineering*. 2016, v. 1, N 1, p. 27-41.
8. Carsten P. Jensen, Kristin K. Madsen, Finn E. Christensen. Small d-spacing WC/SiC multilayers for future hard X-ray telescope designs // *Exp. Astron.* 2005, v. 20, p. 93-103.

Article received 13.11.2017

РОСТ И СТРУКТУРА МНОГОСЛОЙНЫХ РЕНТГЕНОВСКИХ ЗЕРКАЛ WC/Si

Ю.П. Першин, В.С. Чумак, И.Г. Шипкова, В.В. Мамон, А.Ю. Девизенко,
В.В. Кондратенко, М.В. Решетняк, Е.Н. Зубарев

Методами рентгеновской дифракции и просвечивающей электронной микроскопии исследованы особенности роста многослойных рентгеновских зеркал (МРЗ) WC/Si, изготовленных методом прямоточного магнетронного распыления с номинальными толщинами слоев в диапазоне 0,2…30,3 нм (периоды 0,7…38,9 нм). Во всем диапазоне исследуемых толщин слои WC и Si находятся в аморфном состоянии. Установлено взаимодействие слоев WC и Si с образованием силицидов вольфрама (WSi_2, W_5Si_3) и карбида кремния в исходном состоянии. Нижняя перемешанная зона состоит из двух подзон примерно равной толщины. Сделана оценка толщины, плотности и состава всех слоев. На основе определенных параметров предложена пятислойная модель строения МРЗ WC/Si.

РІСТ ТА СТРУКТУРА БАГАТОШАРОВИХ РЕНТГЕНІВСЬКИХ ДЗЕРКАЛ WC/Si

Ю.П. Першин, В.С. Чумак, І.Г. Шипкова, В.В. Мамон, О.Ю. Девізенко,
В.В. Кондратенко, М.В. Решетняк, Є.М. Зубарєв

Методами рентгенівської дифракції та просвічувальної електронної мікроскопії досліджені багатошарові рентгенівські дзеркала (БРД) WC/Si, що виготовлені методом прямоточного магнетронного розпилення з фіксованими швидкостями осадження з номінальними товщинами шарів у діапазоні 0,2…30,3 нм (періоди 0,7…38,9 нм). У всьому діапазоні досліджуваних товщин шари WC та Si являються аморфними. Шари WC та Si взаємодіють з утворенням силіцидів вольфраму (WSi_2, W_5Si_3) та карбіду кремнію в початковому стані. Нижня перемішана зона складається з двох перемішаних підзон приблизно рівної товщини. Зроблена оцінка товщини, щільності та складу всіх шарів. Спираючись на експериментальні результати запропонована п’ятишарова модель будови БРД WC/Si.